Breaking the limitations of visible light communication through its side channel

Cui, Minhao; Wang, Qing; Xiong, Jie

DOI
10.1145/3384419.3430728

Publication date
2020

Document Version
Accepted author manuscript

Published in
SenSys 2020

Breaking the Limitations of Visible Light Communication Through Its Side Channel

Minhao Cui
University of Massachusetts Amherst
Amherst, United States
minhaocui@cs.umass.edu

Qing Wang
Delft University of Technology
Delft, the Netherlands
qing.wang@tudelft.nl

Jie Xiong
University of Massachusetts Amherst
Amherst, United States
jxiong@cs.umass.edu

ABSTRACT

Visible Light Communication (VLC) is a promising technology for future wireless communications. By modulating the visible light—that has about 10,000x larger frequency band than that of radios—to transmit data, VLC has the potential to provide ultra-high-speed wireless connectivities. However, it also has limitations such as i) surrounding objects can easily block VLC links, and ii) intense ambient light can saturate the photodiodes of VLC receivers.

In this work, from a different angle compared with state-of-the-art solutions, we utilize the side channel of VLC—a Radio Frequency (RF) channel created unintentionally during the transmission process of VLC—to break the above-mentioned VLC limitations. The key enabler is that the side RF channel also contains the data information transmitted in the VLC link. When the VLC link is blocked or saturated, we can utilize the side channel, capable of penetrating through blockages and not affected by ambient light, to assist VLC transmissions. Thus a user service relying on VLC transmissions will not be interrupted. Besides the simple Single-Input Single-Output (SISO) case, we consider challenging scenarios where multiple VLC chains are synchronized to form Multiple-Input Multiple/Single-Output (MIMO/MISO) transmission strategies. To make our system practical, we address several challenges spanning from hardware to software. Compared to state-of-the-art design, we reduce the size of the receiving coil by nearly 90%. Experimental evaluations show that our system can decode overlapped RF signals created by a 3×3 MIMO VLC network five meters away, with various blockages in between. Our system also works under intense ambient light conditions (>100,000 lux).

KEYWORDS

Visible light communication, side channel, blockage, saturation, design, implementation

1 INTRODUCTION

While 5G networks are being deployed worldwide, the research competition on 6G technologies has already begun. Visible Light Communication (VLC) is one of the technologies anticipated to be involved in 6G [16, 33], and it has attracted a tremendous amount of attention from both academia and industry. Compared with traditional Radio Frequency (RF) signals such as WiFi and 5G, VLC has several unique advantages: *i) larger frequency band:* compared to the RF band, the visible light frequency band is about ten-thousand times larger,[1] which could potentially enable much higher data transmission rates [19]; *ii) less interference with RF:* located at a much higher frequency band, visible light signals do not interfere with current RF transmissions, mitigating the issue of spectrum crunch [25]; *iii) higher spatial multiplexing:* visible light signals are directional and do not penetrate walls. Therefore the capability of spatial multiplexing is higher compared to RF signals.

As a promising emerging technology, researchers have devoted efforts to improve the throughput, range, and robustness of VLC. There exists a rich literature in increasing the transmission throughput [6, 8, 12, 34, 46, 48]. Besides increasing the light ON/OFF rate to achieve higher throughput, another key concept of increasing throughput is to employ multiple pairs of LEDs and photodiodes to transmit and receive data simultaneously, which is termed Multiple-Input Multiple-Output (MIMO) VLC. If only one photodiode is used to capture multiple LEDs' visible light signals, it then becomes Multiple-Input Single-Output (MISO) VLC. Compared with the mature MIMO/MISO technologies adopted in RF transmissions (e.g., 802.11ac WiFi and 5G), MIMO/MISO VLC is still in its early stage and is attracting a lot of research attentions [4, 5, 20–22, 26].

1.1 Motivation

Though promising, VLC does have several limitations. One critical issue with VLC is that the transmission can be easily blocked by occlusions such as walls, furniture, and even the human itself, as shown in Figure 1. Putting a VLC device in a pocket or bag can fail the transmissions [6, 27, 28]. Other than blockages, another issue with VLC is that the intense ambient light during daytime can significantly degrade the performance of VLC [2, 24, 29]. This

[1] In VLC, the modulation bandwidth depends on the used LED. So far, the modulation bandwidth of off-the-shelf LEDs ranges from several MHz to about 20 MHz. For future advanced LEDs, such as micro-LEDs, their modulation bandwidth can reach GHz [41].

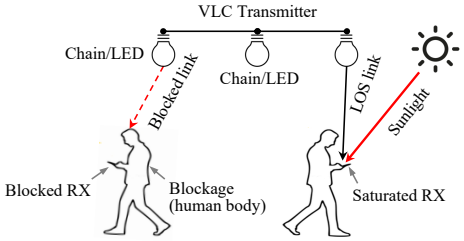

Figure 1: Limitations of VLC systems: (1) visible light signals can be easily blocked by human body, cabinet, etc.; (2) strong ambient light, e.g., sunlight, can saturate VLC receivers.

is because the sunlight's luminance can reach up to 100,000 lux, 100 times larger than that of an LED light for indoor illumination. This intense ambient light can quickly saturate the receiving "antennas" (i.e., photodiodes) at the VLC receiver.

Many recent works have been proposed to combat the above limitations of VLC [10, 32, 39]. To address the blockage issue, a denser deployment that could make sure there always exists a line-of-sight link between the VLC transmitters and the receiver is proposed [4, 5]. Researchers also include human users in the loop to rotate their bodies with the receiver to avoid human body blockage to improve the robustness of VLC [6, 7]. However, these methods either require additional VLC infrastructure [4, 5], or users' cooperation [6, 7]. To mitigate the strong interference from ambient light, a narrow optical bandpass filter is used only to pass the light of intended frequency band [10], and a less sensitive photodetector is adopted to avoid being saturated when ambient light is strong [39]. Although these methods do mitigate the interference to some extent, they sacrifice the large visible light frequency band [10] or can only work when ambient light is not very strong [39].

In this paper, we propose to address the limitations of VLC from a completely new angle, by *employing a radio frequency channel, the side-channel created during the process of visible light communication.* When a VLC transmitter sends data, not just the visible light signal is emitted out, an RF signal is also leaked out [13]. The reason behind this phenomenon is that most VLC systems adopt intensity-based modulations [36] to encode data by quickly turning ON/OFF LEDs. During this ON→OFF/OFF→ON process, the transmitter circuit unavoidably involves a rapid current change in the power line. A changing current induces a changing magnetic field around it. Thus, associated with the VLC channel, *there exists a side RF channel.* In this work, we exploit this side channel to enable a secondary wireless communication. This could overcome the limitations of VLC when there are blockages and/or when ambient light is intense.

1.2 Challenges

The exciting part is that although the light signal can not penetrate through blockages, the side-channel RF signal can get through blockages. It is also not affected by ambient light. Thus, we propose to utilize this side channel to address the blockage and saturation limitations of VLC. The basic idea is that *the side channel contains the data information transmitted in the VLC link.* Thus, when VLC links are blocked, or photodiodes are saturated, we could switch to the side channel for reception. With this idea, the receiver can still receive data without incurring a service interruption. Though

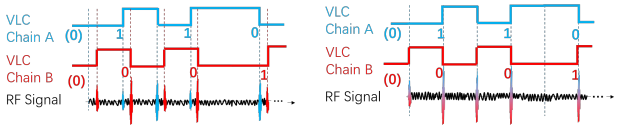

(a) Asynchronous VLC links (b) Synchronized VLC links

Figure 2: Received side-channel signal from two VLC chains.

this side-channel solution sounds promising, to make it practical, several challenges need to be addressed.

- The first challenge is how to design a small receiver to capture the side-channel signal. Existing VLC receivers employ photodiode for light signal reception, and the size of the photodiode can be tiny (0.5cm × 0.5cm). We do not want the added side-channel reception to increase the size of the receiver significantly. On the other hand, the leaked side-channel signal frequency is related to the ON/OFF frequency of the LED and falls in the range of 1-60 MHz (cf. Section 2). To efficiently receive the low-frequency side-channel signal, a large-size antenna is required. To reduce the size of the receiver, people employ coil rather than an antenna for reception. Even with a coil design, the size is still on the scale of a few centimeters [13], too large to fit in the commonly used VLC receivers, especially those small mobile VLC receivers.
- VLC transmitters change the ON/OFF frequency of light to control the data transmission rate, and thus the ON/OFF frequency can vary in a broad range. On the other hand, a coil design (coil size, number of coil turns, etc.) optimized for one frequency may not work well for another frequency. Changing the number of coil turns or the coil size is either inconvenient or even infeasible. It is non-trivial to design a receiver capable of efficiently receiving the side-channel signals in a broad frequency range.
- MIMO VLC is crucial to increase the data rate. MIMO VLC is realized using spatial multiplexing, i.e., multiple transmitters send light signals concurrently towards intended directions [44, 45]. However, when multiple VLC chains send light signals simultaneously, the side-channel signals emitted are not directional. Thus, the side-channel signals are mixed at the receiver and interfere with each other. The recent work [13] proposes to separate mixed side-channel signals in the time domain when multiple VLC links are not synchronized. This is possible because the received signals are sparse and not overlapping in time domain, as illustrated in Figure 2(a). However, in MIMO VLC, the VLC chains (links) are synchronized. Thus, the side-channel signals overlap, as shown in Figure 2(b). In this case, multiple side-channel pulses occur at the same time and interfere with each other. Separating them in time domain is challenging.

1.3 Contributions

To address the first challenge, we use a coil rather than an antenna for signal reception to reduce the receiver's physical size. To further reduce the coil size, we analyze the coil design factors affecting the signal reception. We propose to include the following measures to achieve a smaller size coil while still maintain a good performance

in signal reception: i) adding a magnetic core to *reduce the size of the coil*; ii) utilizing the unique electromagnetic property of coil (Proximity Effect [47] and Skin Effect [47]) to *reduce the number of turns and the thickness of the coil wire, respectively.* With all the measures, we successfully reduce the coil size to a diameter of 2.56 cm without sacrificing the performance. The cost of the coil, together with the magnetic core, is below one dollar.

To address the second challenge, the easiest way is to tune the coil size or the number of turns to receive the side-channel signals at different frequencies efficiently. However, it is unlikely the coil's size can be increased inside hardware with fixed and limited space allocation. To tune the number of coil turns, mechanically moving a probe is inconvenient and slow. We thus propose to include a tunable inductor to address the second challenge. The inductor is connected in parallel with the coil, and the value of the inductor can be controlled by varying the current flow.

To address the third challenge, we consider two different scenarios. Suppose LEDs of different models are used as the transmitter(s). In this case, the mixed side-channel signals can be separated in the frequency domain because the side-channel signals' frequencies are different from each other due to hardware diversity. The more challenging scenario is that the LEDs are of the same model. In this scenario, it is difficult to separate signals in either the time domain or frequency domain. Fortunately, we had one interesting observation through experiments: although the LEDs are of the same model, the RF pulses' time-domain patterns are different from each other. These patterns are unique and stable for each LED. The superposition of these patterns is still unique and can be differentiated. Based on the observation, we design a preamble to obtain all possible time-domain signal patterns when multiple LEDs simultaneously transmit. From the unique time-domain pattern received, we can know which LEDs have ON/OFF transitions and accordingly decode the data from each individual LED even though the side-channel pulses are overlapped.

Combining all the design components, we can successfully utilize the side channel for communication when the VLC links are blocked and/or the photodiodes are saturated. With a cheap coin-size coil design, we demonstrate the feasibility of employing the side channel to deliver the VLC data when the receiver is five meters away with different blockages in between.

Below we summarize the main contributions of this work:

- Based on a recently proposed VLC side-channel model, we design a communication system to address two critical issues of VLC: blockage and saturation. We believe this can be a critical step towards real-life adoption of VLC.
- With theoretical analysis and benchmark experiments, we design a compact and cheap coil receiver to receive the leaked side-channel signals efficiently.
- We observe the uniqueness of the side-channel signals' time-domain patterns and utilize this observation to enable side channel data reception from multiple VLC links.
- We comprehensively evaluate the proposed system by varying the distance, angle, blockage, and ambient light. The results demonstrate that with a small change of preamble at VLC transmitters, by just employing a cheap receiver design, we can significantly improve the robustness of VLC.

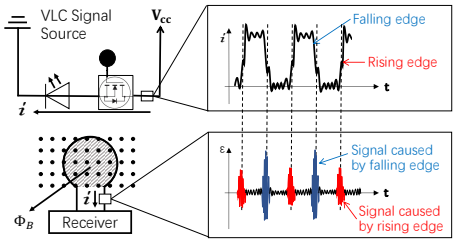

Figure 3: Illustration of the side channel of VLC.

2 BACKGROUND

In this section, we introduce the VLC side channel. For VLC using commercial LEDs, intensity-based modulation is usually used where LEDs are turned ON/OFF to represent data bits "1"s/"0"s. To turn ON/OFF LEDs quickly, the transmitter circuit unavoidably involves a rapid current change. According to Maxwell Equations, a changing current generates a changing magnetic field. With a coil placed around the VLC transmitter, the changing magnetic field induces an electromotive force [35] and this electromotive force can drive the electrons of the coil to generate a current flow. This induced electromotive force can be leveraged to infer the current change at the VLC transmitter, and accordingly, the LED's ON/OFF state for data decoding. That is, there exists a *side channel* associated with VLC that can be exploited to infer the transmitted VLC data, as shown in Figure 3. Because this side-channel signal is low-frequency (1 MHz - 60 MHz), it *can penetrate through obstacles and is not interfered by ambient light.* Due to different frequency range and pulse nature of the signal, the side channel signals do not interfere with RF signals such as Wi-Fi and FM/AM signals.

This interesting side channel of VLC has been modeled and validated in a recent work [13]. Denoting the amplitude of received side-channel signal at the receiver as A_r, it can be expressed as [13]:

$$A_{\mathrm{r}} \propto N \cdot S_{\mathrm{coil}} \cdot \sqrt{G_{\mathrm{res}}(\omega_{\mathrm{s}}, \omega_{\mathrm{r}})}\,, \tag{1}$$

where N and S_{coil} are the number of coil turns and the size (cross section area) of the coil, respectively; ω_{s} and ω_{r} denote the frequency of the side-channel signal and the resonant frequency the receiver, respectively; and $G_{\mathrm{res}}(\omega_{\mathrm{s}}, \omega_{\mathrm{r}})$ is the gain due to the resonance effect.[2] The resonance effect is when the frequency of side-channel signals is equal or close to the intrinsic resonant frequency of the receiver circuit, the amplitude of the received signals significantly increases [9]. For a coil design, the resonant frequency of the receiver ω_{r} could be expressed as [11]:

$$\omega_{\mathrm{r}} \propto \frac{\sqrt{h}}{\sqrt{S_{\mathrm{coil}}} \cdot N}\,, \tag{2}$$

where h is the spacing between adjacent coil turns. To increase the amplitude of the received signal, from Equation (1), we could either match ω_{s} and ω_{r} to obtain a resonance gain, or increase N and/or S_{coil}. However, the coil size S_{coil} and the number of the turns N not only directly determine the amplitude of the received signal A_{r}, but also affect the value of ω_{r}, the resonant frequency of the receiver, and thus indirectly affect the resonance gain [13].

[2]Resonance gain is an energy gain and thus we apply the square root operation to obtain the amplitude gain due to resonance effect.

(a) Small-size coils with different turns

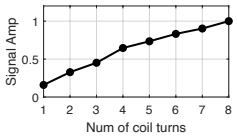

(b) Amplitude increases with N

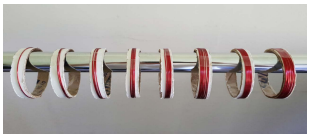

(c) Large-size coils with different turns

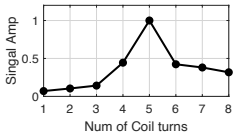

(d) Amplitude does not increase with N

Figure 4: Validating the impact of coil turns on side-channel signal amplitude: (a-b) small coils (diameter: 2.6 cm) and the results; (c-d) large coils (diameter: 7.8 cm) and the results.

To validate the impact of N on A_r, we make two sets of coils with fixed diameter as 2.6 cm and 7.8 cm and with the number of turns varying from 1 to 8 as shown in Figure 4(a) and 4(c). For the transmitter, we use a Function Generator to generate a 20 MHz sine wave current with 40 mA amplitude to drive a 5 mm Chanzon 100F5T LED. For the receiver, we use the hand-made coils. The LED and the receiver coil are 20 cm away from each other and are placed at the same height. Figure 4(b) shows the normalized signal amplitude A_r when varying the number of coil turns. The results validate that the signal amplitude A_r increases linearly with the number of turns N. Figure 4(d) shows the normalized signal amplitude A_r when the coil size is increased to 7.8 cm. We can see that increasing N does not always lead to a higher amplitude of the received signal due to the resonance effect. When $N = 5$, we obtain a larger signal than $N = 8$. Note that when the coil diameter is 2.6 cm, the resonant frequency of the coil is higher than 20 MHz, so we do not have a resonance effect.

3 SYSTEM ARCHITECTURE

We consider the scenario where a VLC transmitter with several LEDs (chains) communicates with one receiver. In the evaluation, we perform both indoor and outdoor experiments. For the outdoor environment, we mainly evaluate our system's performance in tackling the interference from intense ambient light (i.e., sunlight). The LEDs are synchronized and can enable MIMO/MISO VLC between the VLC transmitter and the receiver. Note that when just one LED transmits to one receiver, MISO is simplified as SISO. The surrounding environment has objects that might block the VLC links between the VLC transmitter and the receiver, depending on their relative positions. Mobile objects such as human beings might also become blockages for VLC. The architecture of our system is shown in Figure 5. Below we briefly describe the system components.

VLC transmitter. It modulates several LEDs in each chain to transmit data through visible light channels to a receiver. These LEDs can be co-located or distributed in the area-of-interest. They are synchronized to transmit visible light signals to a single receiver. If the pieces of information sent from each LED are the same, then the receiver can use a photodiode to detect the combined visible light signals from all the LEDs, leading to a MISO VLC. Suppose each LED is modulated to send different data synchronously. In this case, the receiver will need the same number of photodiodes as the number of LEDs to receive and decode the overlapped visible light signals, which is called MIMO VLC. Depending on the LED deployment, we have co-located or distributed MIMO/MISO VLC.

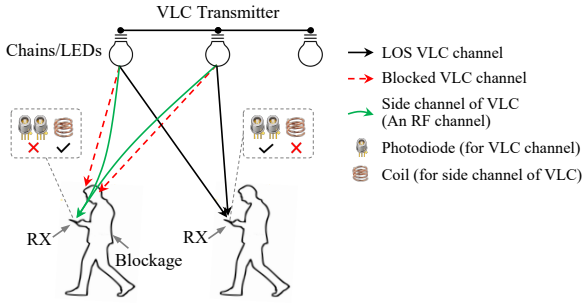

Figure 5: Proposed system architecture. When VLC links are blocked, the RX switches to the side RF links to maintain the connectivity. This switching is *transparent* to the VLC TX.

Blockages. VLC links heavily rely on the line-of-sight (LOS) paths between LEDs and the receiver. If a LOS path is blocked, the communication performance of VLC degrades severely or even wholly fails. In this work, we consider different types of common blockages in our daily life, such as cloth, wall, table and the human body.

Receiver. The receiver in our system is capable of receiving both visible light and the side-channel signals. Besides the photodiodes for light signal reception, a coil built by us is added to capture the side-channel RF signals. When the VLC links are not blocked, the receiver leverages photodiodes to communicate with the transmitter. *If VLC links are blocked or interfered with intense ambient light, the receiver immediately switches to the side RF channels to maintain the wireless connectivity with the VLC transmitter.* Note that this switching process is *transparent* to the transmitter. The key rationale is that the side-channel signals are generated when the VLC transmitters are sending data. Whenever no signals are received from the VLC links, the receiver immediately turns on the side-channel for the reception. If side-channel signals are received, the receiver knows that the VLC links are either blocked or interfered. If there is no side-channel signal, the receiver knows that the VLC transmitter stopped sending data. We could always turn on the side-channel reception at the receiver. However, this operation will consume much more energy.

MIMO and MISO VLC have been thoroughly investigated in the state of the art [4, 5, 21, 22, 26]. In this work, we *only* focus on designing, implementing, and evaluating the proposed system that exploits the side channels of VLC to decode SISO/MISO/MIMO signals transmitted from VLC links. The proposed system can help the receiver maintain wireless connectivity with the VLC transmitter when the visible light links are blocked and/or when the VLC receiver's photodiodes are saturated due to intense ambient light.

4 SIDE-CHANNEL RECEIVER DESIGN

In this section, we present the design of our side-channel receiver. We first present the channel model. Inspired by it, we design a simple circuit that allows us to fine-tune the receiver's resonant frequency. Furthermore, we apply several measures to significantly reduce the coil's physical size while maintaining its performance.

4.1 Side-Channel Model

To achieve a longer transmission range at a lower symbol error rate, we would like to have a larger received signal strength at the coil. As we know, the side-channel RF signal is induced by the changing current at the transmitter. The Maxwell Equations [35] tells us that the amplitude of the induced electromotive force E_F depends on the changing rate of the magnetic flux Φ_B:

$$E_F \propto \frac{d\Phi_B}{dt}. \tag{3}$$

For a fixed time interval, the more magnetic flux changes, the larger the induced electromotive force and accordingly the larger RF signal induced. The amount of magnetic flux could be expressed as:

$$\Phi_B = B \cdot S_{flux} = \mu H \cdot S_{flux}, \tag{4}$$

where B is the flux density of the magnetic field and S_{flux} is the size of the coil the magnetic field passing through. B can be further decomposed as the product of the permeability of the material surrounding the coil (μ) and the magnetic field strength (H). Thus, to increase the magnetic flux, there are three parameters we can tune: μ, H, and S_{flux}. Note that the magnetic field strength H depends on the VLC transmitter, which is not affected by our receiver design. Then, there remain two parameters we can tune to increase the amplitude of the received side-channel signals, μ and S_{flux}. Usually, $\mu = \mu_0$ and μ_0 is the permeability of air. In this work, we propose to add a metal core into the coil to increase the value of μ, which will be detailed in Section 4.3. To increase S_{flux}, we can increase the coil size and the number of coil turns. However, as we target to have a small size coil design, we do not want to increase the coil size or even coil turns.

Besides increasing the value of μ and S_{flux}, another way to obtain a larger amplitude of the received side-channel signal is to match the resonant frequency of the receiver ω_r to the frequency of the side-channel signal ω_s as introduced in Section 2. The general formula to calculate the resonant frequency ω_r of a circuit is as below:

$$\omega_r = \frac{1}{\sqrt{L_r \cdot C}}, \tag{5}$$

where in our design, L_r and C are the inductance and capacitance of the receiver circuit, respectively. When the receiver is just a coil, ω_r can be simplified as Equation (2). If we tune the receiver's resonant frequency through the coil size or the number of coil turns, it will increase the coil size and affect the receiving performance of the coil as shown in Equation (1).

4.2 Fine-Tuning Resonant Frequency

We propose to add an extra inductor in parallel with the coil to vary the inductance L_r of the receiver circuit. By doing this, we do not need to tune the coil but can still tune the resonant frequency. The inductance of the whole receiver L_r after paralleling the inductor can be expressed as:

$$\frac{1}{L_r} = \frac{1}{L_{coil}} + \frac{1}{L_{extra}}, \tag{6}$$

where L_{extra} is the inductance of the added inductor.

To validate our method, we conduct experiments with the paralleling inductor, as shown in Figure 6(a). In the experiment, we place different inductors in parallel with the coil to tune the receiver's inductance. The results are shown in Figure 6(b). We can observe that paralleling the inductor and varying its value changes the receiver's resonant frequency. The higher inductance of the inductor, the lower the resonant frequency of the whole receiver circuit. Therefore, with the added inductor, we can successfully tune the receiver's resonant frequency without touching the coil design. As described in Section 4.1, the frequency of the side channel signal is unknown in advance. To measure the frequency of the side channel signal (the resonant frequency of the transmitter) at the receiver side, we tune the receiver coil's frequency by changing the current flow inside the paralleled inductor as detailed above. When the largest signal amplitude is reached, the side channel signal frequency equals to the receiver resonant frequency.

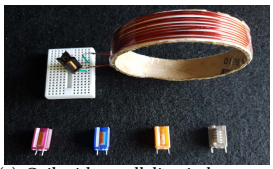

(a) Coil with paralleling inductors with different inductance

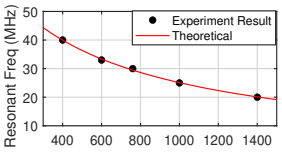

(b) Resonant frequency vs. paralleling inductors with different inductance

Figure 6: Experiment with paralleling inductors.

4.3 Designing a Small Coil for Signal Reception

Expression of the resonance gain. The amount of resonance gain measures the signal amplitude increase when the receiver's resonant frequency matches the signal frequency [15]:

$$G_{res}(\omega_s = \omega_r) \propto \frac{\omega_s}{R_r}, \tag{7}$$

where R_r is the resistance of the receiver. Since ω_s is the frequency of the side-channel signals which could not be tuned, the only parameter left that we can use to tune the resonance gain is the resistance of the receiver R_r. Substituting Equation (7) into Equation (1), we obtain:

$$A_r \propto \frac{N \cdot S_{coil} \cdot \sqrt{\omega_s}}{\sqrt{R_r}}. \tag{8}$$

Inspired by the model presented in Section 4.1, we propose three measures that can be leveraged to reduce the physical size of the receiver coil.

4.3.1 Reduce the coil size (S_{coil}) without sacrificing the magnetic flux (Φ_B) passing through. From Equation (4), while H is decided by the transmitter, we have two parameters to tune at the receiver side: S_{coil} and μ. Note that if we want to decrease the value of S_{coil} while still maintaining the magnetic flux, we need to increase the value of μ. For just a coil, the surrounding material is air, which has a small μ. We thus propose to insert a magnetic core with a large μ in the coil. By doing this, we increase the value of μ, so the amount of magnetic flux is not decreased if we decrease the coil size S_{coil}. In our design, we choose the ferric oxide as the core material, which is cheap and often used in AM radio antenna design. Through experiments, we find that a copper coil with a diameter of 2.54 cm and ten turns wired around a ferric oxide core can achieve the same performance in signal reception as a copper coil, which has ten turns and a diameter of 7.8 cm without the ferric oxide core.

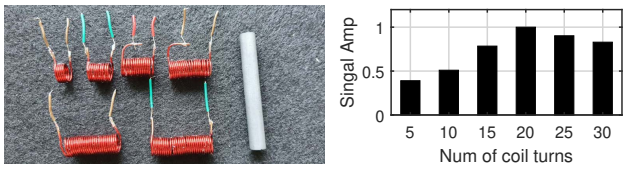

(a) Small coils with turns from 5 to 30 (b) Signal Amp vs. turns of coil

Figure 7: Experiment with different turns of the small coil: (a) The coils; (b) Results.

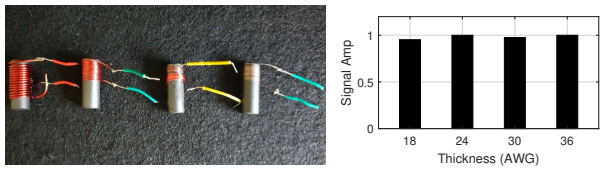

(a) Coils with wire of different thickness (b) Signal Amp vs. wire thickness

Figure 8: Experiment with different wire thickness and materials of the small coil: (a) The coils; (b) Results.

This result shows that adding a ferric oxide core can reduce the receiver coil size by nearly 90%.

4.3.2 Optimize the number of the turns of the coil. After reducing the coil size S_{coil}, our next step is to optimize the coil's turns. According to Equation (8), using a coil with more turns (N) will linearly increase R_{r}. However, because only the square root of R_{r} contributes to the amplitude, increasing the number of turns increases the amplitude of the received signal slowly. However, this is not true in reality. We conduct experiment to measure the signal amplitude when we increase the number of coil turns. From the results shown in Figure 7(b), we can tell that the amplitude of the received signal does not always increase with the number of turns.

The reason behind this phenomenon is the Proximity Effects [47]. The current in the nearby coil will influence each other's current flow. The direct result of the Proximity Effect is that the resistance of the coil increases *exponentially* with the number of coil turns. Initially, when we increase N from 5 to 20, the benefit of increasing N dominates compared with the Proximity Effect. However, when N further increases, the Proximity Effect dominates, inducing a significantly larger R_r and reducing the signal amplitude. The Proximity Effect is verified in our experiment, and there exists an optimal number of turns which can achieve the best reception performance. The optimal N value can be measured through experiments.

4.3.3 Reduce the thickness of the coil wire. We further reduce the coil size by choosing a thinner wire. The coil's resistance, R_{r}, which affects the amplitude of the received side-channel signal, is closely related to the thickness of the coil wire. We employ coils made of different thicknesses of wires as shown in Figure 8(a) to validate the impact of the wire thickness on the received signal's amplitude. The results are shown in Figure 8(b). We can see that the result is not as expected that the thicker wire presents us a stronger signal. The thickness of the wire actually has little effect on the amplitude of the signal. This is due to another effect of the coil, Skin Effect [47]. As a result, the amplitudes of the received side-channel signals

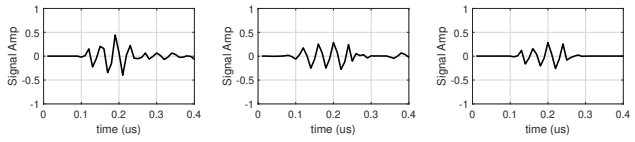

(a) Side-channel signal generated by LED A (b) Side-channel signal generated by LED B (c) Side-channel signal generated by LED C

Figure 9: Observation 1: the envelopes of side-channel signals generated by LEDs of the same model are unique.

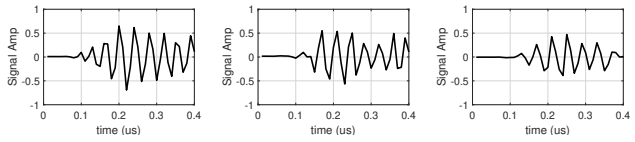

(a) Superposed RF signal from LEDs A and B (b) Superposed RF signal from LEDs A and C (c) Superposed RF signal from LEDs B and C

Figure 10: Observation 2: the superposed side-channel RF signals from multiple LEDs are also unique from each other.

are similar to each other. In this work, we leverage this insight to design a coil with thin wires to further reduce the receiver coil's size without sacrificing the signal reception performance.

5 DECODING SIDE-CHANNEL DATA

In this section, we first present two observations from our experiments. Then, based on these observations, we propose decoding methods for SISO/MISO/MIMO transmissions.

We randomly select three out of the ten homogeneous LEDs (Kapata 5W) in the lab for experiments. We put them in three VLC chains and configure all the chains to send synchronized signals from the VLC transmitter to the receiver. Three side-channel signals are also generated during this process, and the designed receiver captures these RF signals. Depending on the three LEDs' ON/OFF states, we can receive different combinations of the receiver's side-channel signals. We repeat the above process with varying LED combinations for multiple times. From the results, we observe *two* essential properties of the side-channel signals.

Observation 1: *The envelopes of the received side-channel signals generated by different VLC chains are unique in the time domain.* We observe that even LEDs of the same model are used, the envelopes of the generated side-channel signals are still unique, as illustrated in Figure 9. This is because even though the LEDs are of the same model, there are still tiny differences in the hardware. These differences contribute to our observed result that the envelopes of the side-channel signals generated by LEDs of the same model are unique even though the frequency of the generated side-channel signals is almost the same. Moreover, the envelopes are stable over time.

Observation 2: *The envelopes of multiple superposed signals are also unique and stable.* The side-channel signals generated by multiple VLC chains are additive at the receiver. More importantly, the envelopes of the superposed signals are also unique. This phenomenon is shown in Figure 10, from which we can observe that the superposed side-channel signals are unique. This is because the

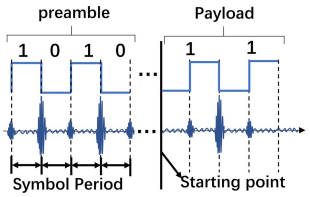

Figure 11: Preamble and payload.

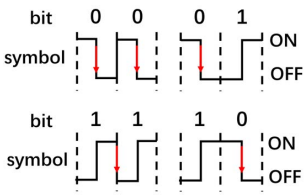

Figure 12: Decoding with falling edges.

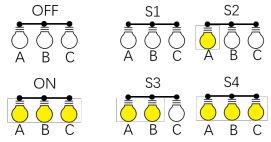

(a) 2 levels (b) 4 levels

Figure 13: Multi-Level modulations.

side-channel signals are electromagnetic signals, which meet the requirement of field superposition [14].

Based on these two observations, we continue to present how to decode data in the side-channel signals.

5.1 Decoding MISO/SISO Data

Multiple chains of a VLC transmitter can be configured to send the same data in a synchronized manner, leading to MISO transmissions. When there is just one VLC chain enabled, the transmission is called SISO. When multiple VLC chains are enabled and configured to send the same data in a synchronized manner, there will be only two states, i.e., all the LEDs of multiple chains are ON, or all the LEDs of multiple chains are OFF, as illustrated in Figure 13(a). Further, from *Observation 2*, we know that multiple side-channel signals are additive and lead to a unique and stable superposed signal. Thus in MISO, we only have one stable and unique superposed side-channel signal: the superposition of all the side-channel signals generated by all the VLC chains. For the receiver, from the decoding point of view, there is thus no difference between the side-channel signals generated from MISO VLC and SISO VLC. Below we present the side-channel decoding method that works for both MISO and SISO.

As illustrated in Figure 3, when the light is turned ON and OFF, ideally, the current flow changes like a square wave with rising edges and falling edges. The rising/falling edges of the changing current at each VLC chain induce changing electromagnetic fields. These changing electromagnetic fields induce an electromotive force in the coil, which is the received side-channel RF signal. One property of this RF signal can be leveraged to decode the VLC transmission is that: *The strengths of the side-channel RF signal induced by the raising edge and by the falling edge are very different and thus distinguishable.* For example, for a widely used commodity LED (Kapata 5W LED), the side-channel signal has a larger strength when the LED is switched from ON to OFF (falling edge) than from OFF to ON (rising edge). A snapshot of this property obtained from experiments is also shown in Figure 11.

To differentiate the side-channel signals from the noise, we apply the Hilbert-Huang transform [23] on the raw captured signals to obtain the instantaneous energies of the intrinsic mode functions of the raw signals. The raw signals are shown in Figure 14(a), and signals after the Hilbert-Huang transform are shown in Figure 14(b). We could see the difference between the side-channel signal and the noise. Then, we sum up the side-channel signal's calculated energy and the noise over a fixed window size based on the Hilbert-Huang transform. The results are shown in the Figure 14(c). We can use a threshold-based method to filter out the noise. With the above denoising method, we can significantly increase the communication range of the side channel of VLC. The corresponding experiment results are presented in Section 7.

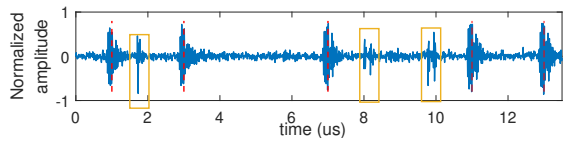

(a) Raw signals with red line as intended signal and noise in yellow rectangles

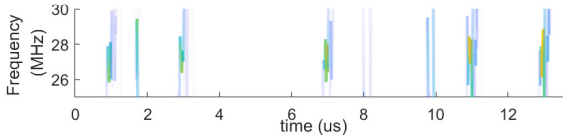

(b) Signals after Hilbert-Huang transform

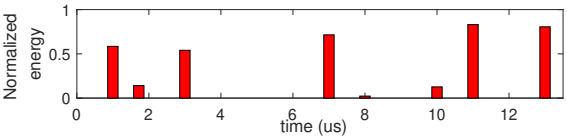

(c) Calculated energy based on the transformed signal

Figure 14: Denoising the side-channel signals using Hilbert-Huang transform.

Preamble detection and symbol period. To decode a frame from the captured signal, we first need to detect the preamble and calculate the symbol period. A commonly used preamble in VLC is a list of consecutive alternating ON/OFF symbols [17, 18, 38], as shown in Figure 11. The rising/falling edges appear at the ON→OFF and OFF→ON transitions, respectively. Therefore, during the preamble transmission, a list of consecutive alternating small/large signals (caused by rising/falling edges, respectively) can be captured by the side-channel receiver. This repeating small/large signal pattern can be easily exploited to detect the preamble. After that, from the detected preamble we can know the symbol period and the starting point of the payload.

Decoding data by only exploiting the falling edges. For decoding the data, we decide only to leverage the side-channel signal induced by the falling edge because it has a larger strength than the signal induced by the rising edge and thus could bring us a longer communication distance. Note that when the distance between the side-channel receiver and VLC transmitters is larger than three meters, the signal induced by the rising edge is overwhelmed by noise. In contrast, the falling edge induced signal can still be detected at 5-6 m. Thus if we can decode the data by using just the falling edge, we can achieve a much larger transmission distance.

However, this is challenging because we only use half the received signals (by dropping the side-channel signals induced by the rising edges) for decoding. To overcome the challenge, we exploit

the Manchester coding, which is usually used in VLC to solve the flickering problem [13]. We design a decoding algorithm that decodes two bits (i.e., four symbols) at a time. For each combination of the two bits (00, 01, 10, and 11) at the transmitter, they either have a different number of falling edges and/or these falling edges appear at different positions: 1) for 00, there are two falling edges at the transitions between the first and the second symbols, and between the third and the fourth symbols, respectively; 2) for 01, there is one falling edge that is after the first symbol; 3) for 10, there is one falling edge that is after the third symbol; and 4) for 11, there is one falling edge that is after the second symbol. This observation is visualized in Figure 12. By detecting the number of signal instances generated by the falling edges and their relative positions, we can distinguish all the four possible bit combinations 00, 01, 10, and 11.

5.2 Decoding MIMO Side-Channel Data

The multiple chains at a VLC transmitter can also be leveraged to transmit different data streams, creating multiple side channels through which different RF signals are transmitted. When multiple chains are synchronized to transmit data, it can form a MIMO VLC network. If they are not synchronized, then they become multiple SISO VLC links. We continue to present how to decode these multiple side-channel signals at the receiver.

As presented in Section 3, for decoding multiple side-channel signals, it is more challenging when the VLC chains are synchronized than the scenario when they are not synchronized. When multiple chains are not synchronized, we can separate multiple side RF signals in time domain (cf. Figure 2(a)). However, when multiple LED chains are synchronized to enable MIMO VLC, their generated side-channel signals are *overlapped at the receiver* in time domain. Thus, they can not be easily separated in *time domain*. If MIMO VLC uses different models of LEDs in the front-end, we could differentiate the overlapped side-channel signal in frequency domain because the frequencies of the side-channel signals are different due to the electric characteristics of different models. However, this solution will fail when homogeneous LEDs (LEDs of the same brand and same model) are used in MIMO VLC, which is the common case, the frequencies of their generated side-channel signals are very similar. This can be seen clearly from our measurement results shown in Figure 15. As a result, the above differentiating solution does not work. Therefore, it is also challenging to separate and distinguish the overlapped side-channel signals generated by homogeneous LEDs in *frequency domain*.

To decode the MIMO VLC transmissions through the side channels, we need to know each slot of the side-channel signals generated by VLC chains. We could not separate them in frequency domain since the side channel signals generated by the same Model LEDs have the same frequency feature. We could not separate them in time domain neither since they overlap with each other. The two observations presented at the beginning of Section 5 tell us that the side-channel signals' envelopes, no matter from a single side channel or the superposition of multiple side channels, are all unique and stable. Thus we propose to use the Dynamic Time Warping (DTW) method to measure the similarity between signals and classify them to decode the information.

For classifying, we add a new preamble part at the VLC transmitter to include the signal patterns of all possible combinations of

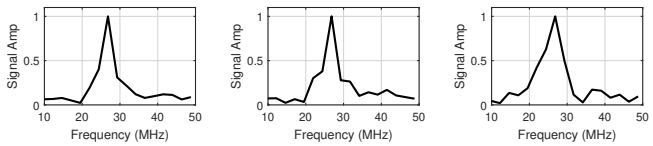

(a) Side-channel signal generated by LED A (b) Side-channel signal generated by LED B (c) Side-channel signal generated by LED C

Figure 15: The frequencies of the side-channel signals generated by homogeneous LEDs.

LEDs to help the receiver determine which VLC chains are transmitting. The VLC chains are synchronized and have the same data rate. For a transmitter with three VLC chains denoted as CH_A, CH_B, and CH_C, we employ eight (2^3) slots in the preamble part to embed the patterns of all possible combinations of LED transmissions. None of the three LEDs transmits in the first slot, and it is denoted as $\{\emptyset\}$. In the second slot, we only let CH_A transmit, and it is denoted as $\{CH_A\}$. In the third slot, we only let CH_B transmit. We continue this process to have all combinations of the three transmitters. In the last slot, we let CH_A, CH_B, and CH_C all transmit. At the receiver side, by looking into the preamble part, we obtain eight patterns which cover all possible combinations of LEDs: $\{\emptyset\}$, $\{CH_A\}$, $\{CH_B\}$, $\{CH_C\}$, $\{CH_A, CH_B\}$, $\{CH_A, CH_C\}$, $\{CH_B, CH_C\}$ and $\{CH_A, CH_B, CH_C\}$. We can then employ these eight patterns to decode each slot in the data part and know which chain(s) is transmitting. Such a look-up-table-based method is simple but efficient. Once we distinguish the signals from each side-channel, we can continue to use the decoding method presented in Section 5.1 to decode data.

One issue with this method is that the number of preamble slots grows exponentially with the number of the transmitters. However, we want to point out that we do not need to add this designed preamble part to every packet because these patterns are stable in a short period. Thus, we need to send one packet with the designed preamble periodically. If the receiver is not moving, from our experiments, the patterns are stable for tens of seconds.

5.3 Decoding Multi-Level Side-Channel Data

Another interesting scenario is multi-level VLC modulation, where the status of each symbol can change between multiple states instead of the two states ON and OFF, as illustrated in Figure 13(a). Here the LEDs are co-located, which is usually used in the state of the art such as [42, 43] to improve the data rate of VLC while avoiding the non-linear property of LEDs. To decode the data, *we only need to justify how many LEDs are currently ON, i.e., how many chains contribute the side-channel signal at the considered time slot.*

Using a 4-level VLC modulation as an example. It can be enabled at a VLC transmitter that has three chains (LEDs) as CH_A, CH_B and CH_C. We use S1, S2, S3, and S4 to denote the four possible states of each symbol, as shown in Figure 13(b). S1 is achieved by turning off all the LEDs; S2, S3, and S4 are achieved by turning on one, two, and three LED(s), respectively. According to *observation 2*, the multiple side-channel signals are additive at the receiver, and the superposed signals are unique. To decode the data, we can use similar methods introduced in the MIMO scenario. The only difference is that now we do not need to employ eight slots in the preamble to embed the

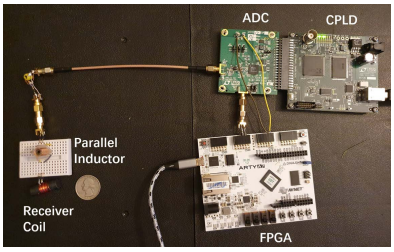

Figure 16: Our implemented receiver.

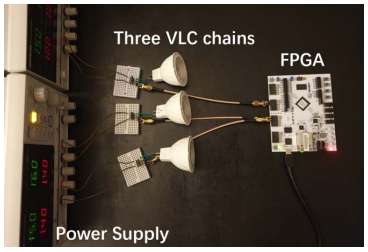

Figure 17: Centralized VLC chains/LEDs.

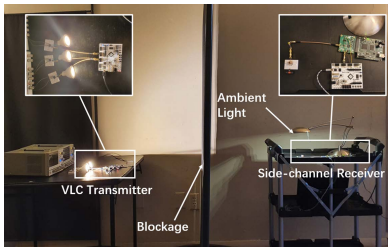

Figure 18: Basic experimental setup.

patterns of all the possible combinations of the LEDs. Instead, we only need to use four slots to embed four combinations of the LEDs: $\{\emptyset\}$, $\{CH_A\}$, $\{CH_A, CH_B\}$ and $\{CH_A, CH_B, CH_C\}$. The rest of the decoding is the same as that presented in Section 5.2 for decoding the MIMO side-channel signals.

6 IMPLEMENTATION

In this section, we present the implementation of our side-channel receiver as well as the VLC transmitter.

Side-channel receiver. We implement the receiver with off-the-shelf hardware components. A snapshot of the receiver is shown in Figure 16. It consists of three main components: i) a small and cheap (less than one dollar) coil that can be fine-tuned to receive the side RF signals; ii) an Analog to Digital Converter (ADC) to sample the RF signals received at the coil; and iii) a Complex Programmable Logic Device (CPLD) to collect and transmit the signal samples to a laptop for further processing. The coil is built with the wire of 30 AWG (American Wire Gauge) [1] wrapping around a ferric oxide core. The coil is paralleled with a variable inductor (Coilcraft 143-20J12L) whose inductance value can be adjusted to fine-tune the resonant frequency of the receiver. The number of the coil turns is 20, which is an optimal value according to our measurements. The diameter of the coil is 2.54 cm. Compared to the state-of-the-art coil design in [13], we reduce the coil size by 90%. The ADC we use is LINEAR LTC2208, which has a 100 MHz sampling rate, enough to sample the received RF signals from the VLC transmitters. The CPLD adopted is LINEAR DC718. Finally, we employ Matlab, hosted on a Thinkpad X1 carbon laptop with an Intel i7 CPU and a 16G memory, to process the signal and decode the data.

VLC transmitter. We build a transmitter that flexibly supports various numbers of VLC transmitting chains. We design a circuit for each chain to drive a commercial Kapata 5W LED separately. We program an FPGA Arty A7 to control each VLC transmitting chain to send out visible light signals. Depending on the application scenarios, our system can flexibly configure the transmitting chains to support SISO/MISO/MIMO transmissions. The basic modulation scheme we use is On-Off-Keying (OOK) with Manchester Coding. In each enabled chain, the LED is turned ON/OFF at a frequency of 1 MHz, same as the latest version of the popular open-source VLC platform OpenVLC [17]. In one of the experiments, we also employ three chains to implement a multi-level (4-level) modulation scheme for evaluation.

7 EVALUATION

In this section, we present the performance evaluation of our system in various scenarios.

Setup and metrics. As shown in Section 6, we use the commercial Kapata 5W LEDs at the VLC transmitter. Based on our measurement, we configure the inductance value of the variable inductor Coilcraft 143-19J12L to 1440 nH to match the resonant frequency of our receiver with the frequency of the side-channel signals induced by the VLC transmitter. We use *Symbol Error Rate (SER)* as the main performance metric. Following recent work on VLC [37], we employ *transmission range* as the other metric in the evaluation, which is defined as the maximal communication distance with an SER below 10^{-2}. Since the data carried in the side RF channel is the same as the data carried in the VLC channel, we could employ the same error correction scheme adopted in the VLC channel to correct errors in the RF side channel.

7.1 Co-Located VLC LEDs

In this scenario, all the chains (LEDs) of the VLC transmitter are co-located. We place the side-channel receiver at the same height as the VLC transmitter. *A piece of thick cloth is deployed between the transmitter and the receiver as a blockage* to block their line-of-sight VLC links, as shown in Figure 18.

MISO/SISO transmissions. The decoding process of MISO/SISO transmissions is the same for our side-channel receiver. Due to the space limit, here we only present our evaluations on decoding MISO transmissions. In the MISO case, all the chains are configured to send the same data synchronously. We use our receiver to capture the side-channel signals at different distances, ranging from three meters to six meters at a step size of 0.5 m. After we receive the raw side-channel signals, we denoise and decode the data in them with the proposed methods presented in Section 5.1. The achieved SER results are shown in Figure 19. As a comparison, we also show the SER when the raw signals are not denoised. We can observe that although the SER increases when the distance increases, our side-channel receiver can achieve SERs below 10^{-2} at all the tested distances. When the distance is 3 m, the achieved SER even goes as low as 10^{-5}. Our proposed denoising method also significantly improves the performance of the side-channel receiver. For example, at the distance of 3 m, when the signals are not denoised, the SER is 10^{-2}; after we denoise the signals, the SER is decreased to 10^{-5}.

MIMO transmission. In this case, the VLC chains of the transmitter are configured to send different data simultaneously. We use our receiver to capture the side-channel signal at distances beginning from three meters to five meters at a step size of 0.5 m. The proposed differentiating and decoding methods detailed in Section 5.2 are used to process and decode the data. In this experiment, we employ 2×2 MIMO to demonstrate the feasibility. The SER for

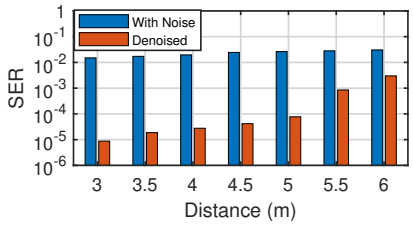

Figure 19: Symbol error rate of the side channel for MISO transmissions.

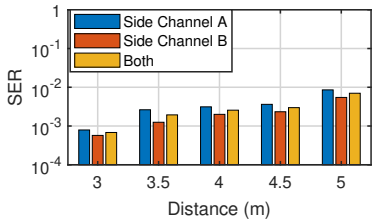

Figure 20: Symbol error rate of the side channel for MIMO transmissions.

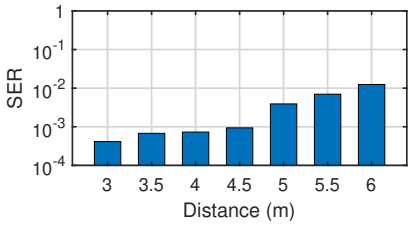

Figure 21: Symbol error rate of the side channel with multi-Level modulation.

(a) Examples of the blockages

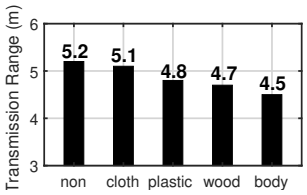

(b) Transmission range vs. blockages

Figure 22: Evaluation with different blockages: (a) Examples: plastic, 2 cm wooden table, and a human body; (b) Results.

each side channel and the overall MIMO[3] are shown in Figure 20. We can see that the SER increases with increasing distance. The transmission range is shorter than the transmission range of MISO since the required signal amplitude to decode MIMO VLC is larger in order to differentiate different combinations of the two side-channel signals as detailed in Section 5.2. In the MIMO scenario, we can still achieve an acceptable performance (smaller than 1% SER) at a distance of five meters.

Multi-level modulation. Next, we evaluate the side channel's performance when the 4-level modulation is adopted at the VLC transmitter. The experiment setup is almost the same as the MISO scenario. The only difference is that we use the number of lighting LEDs to modulate data as detailed in Section 5.3, instead of all of the LEDs sending the same data. Therefore, the four levels are achieved by turning off all the LEDs and turning one LED, two LEDs, and three LEDs. The SER results are shown in Figure 21. The SER increases with the distance and the achieved transmission range is about 5.5 m.

Different blockages. We also evaluate the system's performance with various blockages between the VLC transmitter and the side-channel receiver. We use common blockages in our indoor environments, including a piece of cloth, a table made of plastic, a table made of wood, and a human body. These blockages are shown in Figure 22(a). We use the same setup shown in Figure 18 for this experiment. The MIMO transmission results are shown in Figure 22(b). We can observe that the blockages do affect the performance of the side-channel communication. For example, with a cloth as the blockage, the transmission range is 5.1 m while this value decreases to 4.5 m for a human body blockage. Nevertheless, 4-5 m is an acceptable range considering that the VLC transmission distance is also usually several meters. When there is a blockage such as a table or a human body, the VLC links are blocked.

[3]Note that the overall SER performance is the average of the SERs of the two channels.

7.2 Distributed VLC LEDs

We also conduct experiments to evaluate the performance of our system with distributed LEDs. We deploy the VLC LEDs at different locations to enable distributed MIMO/MISO transmissions under these scenarios. We test our system in two representing environments: a corridor and a living room. *A piece of thick cloth is also deployed near the receiver as a blockage* to prevent it from receiving light signals from any chains of the VLC transmitter.

Corridor environment. A snapshot of the setup is shown in Figure 23(a). The corridor has a length of four meters and a width of one meter. We place the two LEDs at positions $(2m, 0.5m)$ and $(3m, 0.5m)$ as shown in Figure 23(b). The two chains are controlled to send synchronized and different visible light signals, enabling 2×2 MIMO VLC transmissions. We place our side-channel receiver at 27 different locations with a spacing of 0.5 m between adjacent locations in the area-of-interest, as marked as red dots in Figure 23(b), to evaluate its performance. Furthermore, we move the receiver to the adjacent kitchen and consider four additional receiver locations, as shown in Figure 23(a). When the receiver is in the kitchen, there is *a concrete wall blockage* between the receiver and the VLC transmitter. We use the differentiating and decoding method detailed in Section 5.2 to process and decode the data because the proposed method works for both co-located and distributed LEDs. The obtained SERs of the two side channels are shown in Figure 23(c) and 23(d), respectively. The average SER of the two channels is shown in Figure 23(e). For all the positions in the corridor, we could get an average SER around 10^{-3}. The worst SER is 3×10^{-3}, well below the acceptable threshold of 10^{-2}. The average SER in the kitchen is 4×10^{-3}, worse than that in the corridor due to the impact of the concrete wall. However, it is still below the threshold of 10^{-2}.

Living room. We also carry out experiments within an area-of-interest of 3 $m \times 3$ m in a living room. We enable all the three transmitting chains and deploy them in a triangular topology at positions $(0.75\ m, 0.75\ m)$, $(2.25\ m, 0.75m)$, and $(1.5\ m, 2.25\ m)$, respectively, as shown in Figure 24(a). The three chains are controlled to send data streams synchronously, leading to 3×3 MIMO VLC transmissions. We test our side-channel receiver's performance at 36 different positions at a step size of 0.6 m, indicated by the red dots in Figure 24(a). The achieved average SER for all the three side channels is presented in Figure 24(e). Moreover, we also calculate the SER for each side channel and the results are shown in Figure 24(b), 24(c), 24(d). The achieved average SER is 3×10^{-3}, which is lower than the threshold of 10^{-2}. We also notice that the side-channel receiver performs better at positions near the VLC chains

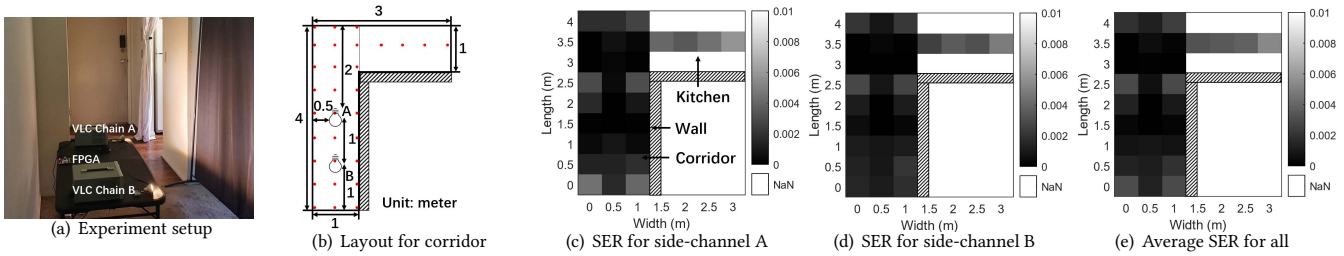

(a) Experiment setup (b) Layout for corridor (c) SER for side-channel A (d) SER for side-channel B (e) Average SER for all

Figure 23: Evaluation in corridor: (a) shows the experiment scenario in the corridor and kitchen; (b) experiment layout for the corridor and kitchen; (c-d) the calculated SER at different positions for the two side channels, respectively; (e) the average SER at different positions.

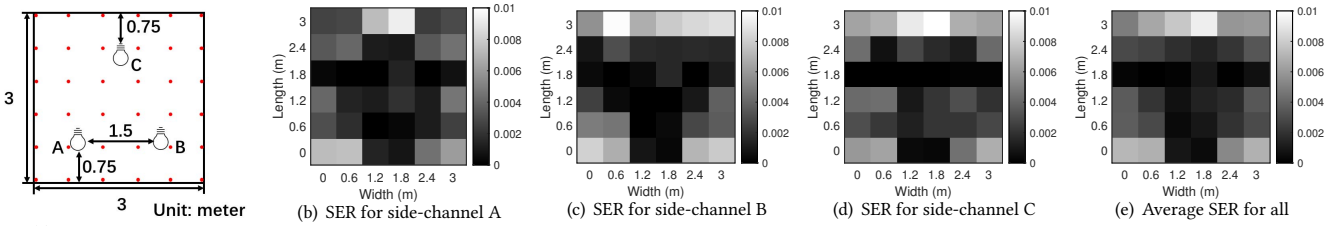

(a) Layout for living room (b) SER for side-channel A (c) SER for side-channel B (d) SER for side-channel C (e) Average SER for all

Figure 24: Evaluation in living room: (a) experiment layout for the living room; (b-d) the calculated SER at different positions for each side channel, respectively; (e) the average SER at different positions.

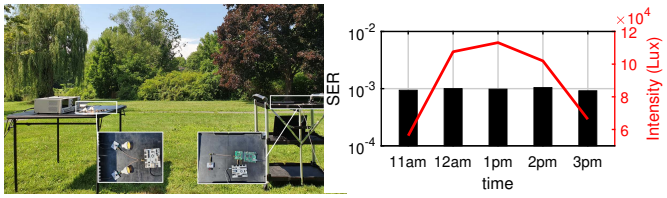

(a) Outdoor setup (b) SER vs. different time in a day

Figure 25: Outdoor evaluation: (a) setup; (b) SER result.

since the signals' amplitudes are larger and therefore provide more details for differentiating multiple side-channel signals.

From both the corridor and living room scenarios, we notice that the angles between the VLC transmitter (more specifically, the LEDs at each transmitting chain) and the side-channel receiver do not affect the receiving performance. This is because the side-channel RF signals emitted from the VLC transmitter are omnidirectional, as presented in Section 2. We also notice that the overall performance of the distributed MIMO VLC is better than that of the co-located MIMO VLC. The main reason is that to decode the received data successfully, we not only need to capture the signal but also need to differentiate the signals between each side channel, as presented in Section 5. In distributed scenarios, the large inter-LED distance of different transmitting chains introduces more difference in the side-channel receiver's overlapped signals, which helps differentiate signals among different side channels.

In the corridor and the living room, we also test our receiver's performance when the transmitter configures its VLC chains to form MISO transmissions. The achieved SERs at the side-channel receiver at all the locations are always smaller than 10^{-3}, which are adequate for wireless communications through the side channels when VLC links are blocked.

7.3 Outdoor Scenario

Strong ambient light such as sunlight can saturate the photodiode of the VLC receiver easily. To test the performance of our receiver under strong ambient light conditions, we carry out experiments in outdoor environment five times between 11 am to 3 pm. During this period, the sunlight is usually the strongest. We measure the intensity of the ambient light with the APP "Light Meter" hosted by a smartphone SAMSUNG Galaxy S10. We also use SER as the performance metric. The evaluation results are shown in Figure 25(b). The measured ambient light is very strong, with an intensity varying from 56,000 lux to as high as 114,000 lux. Under this level of ambient light, the photodiode at a VLC receiver is easily saturated, as pointed in the state of the art [10, 40].[4] However, we can see clearly from the results that the SER achieved at our side-channel receiver is around 10^{-3} in all the five tests under different levels of ambient light. This result shows that our side-channel receiver works well under strong ambient light scenarios and can help maintain communication connectivity when the photodiode is saturated.

8 DISCUSSIONS

Limitations of the system. Currently, the proposed receiver design works well when the number of LEDs in the VLC transmitter is up to 3. When we further increase the number of LEDs, the performance degrades. This is because the number of possible combinations increases exponentially with the number of LEDs. With more possible combinations, the difference among each combination becomes smaller, and thus it is more challenging to differentiate among the combinations. We believe advanced machine

[4] We also perform some tests and find the photodiode SFH206K adopted in OpenVLC 1.3 is already saturated when ambient light intensity reaches 20,000 lux.

learning techniques such as support vector machine and convolutional neural network can be applied to improve the capability of differentiating different combinations and accordingly increase the number of simultaneous LED transmissions. Furthermore, when we utilize the side RF channel to assist high-data-rate VLC systems, we need to replace the coil with other appropriate types of antennas because the frequency of the side-channel signal generated by these high-data-rate VLC systems is also higher.

Solutions that are non-transparent to LED transmitters. In this work, except for that we need to modify the preambles at the transmitter, our solution is transparent to the LED transmitters. The LED transmitters do not need to know when the VLC links are blocked and when the receiver is receiving the transmitted information through the side RF channels. However, the LED transmitters could also be modified to increase the amplitude of the side RF signals. There are several ways to enlarge the side RF signals, such as increasing the power line's length in the circuit, increasing the amplitude of the current in the circuit, and enabling faster light ON/OFF switching (i.e., make the current change faster). Although these methods can make side RF channel work better, they will unavoidably affect the original transmissions on the visible light channels. Therefore, a trade-off exists between the side RF channel and the main light channel when the VLC transmitter circuit is modified.

Potential applications. The side RF channel could also enable other applications besides communications. The first possible application is Visible Light Position (VLP), a promising application built upon visible light communication. In VLP, receivers use the visible light signals transmitted from the transmitters for localization. However, VLP also suffers from blockage and ambient light saturation. With the side RF channels, we could use the RF signals' amplitudes for positioning based on traditional positioning methods such as triangulation, even when the VLC links are blocked or interfered with ambient light. Another possible application is to leverage the side RF channel for human activity sensing. We believe that the side RF channel can also assist visible light sensing because the information from another dimension is now available.

9 RELATED WORK

VLC side channel. The side RF channel of VLC was first exploited and modeled in a recent work [13] to perform a sniffing attack. In this work, we utilize the side channel to assist the communication of visible light. Besides different motivations, we improve the side RF channel model as well as the receiver design as follows: i) We improve the side channel model by including the skin effect and proximity effect into the model; ii) We improve the design of the coil by reducing its physical size by 90% so it can be fit into the VLC system without requiring a significant amount of extra physical space; iii) We design a circuit to perform the resonant frequency matching in software, instead of mechanically tuning the coil in [13]; iv) We realize MIMO/MISO communication using the side RF channel by designing a new wireless communication scheme based on the unique patterns of the preamble.

Blockage in VLC. We know that visible light cannot pass through non-transparent blockages. Therefore, it is always challenging to achieve a reliable VLC system because surrounding mobile/stationary objects can easily block the LOS links. To tackle this problem, researchers have proposed methods in three dimensions: at the transmitter side [4, 5], the propagation channel [49], and the receiver/user side [6]. To reduce the probability of a VLC link being blocked, the authors in [4, 5] propose to deploy dense VLC transmitters to avoid the blockages. However, such a dense architecture increases the deployment cost of the infrastructure. Receivers could also use the reflected light signals to decode the data when the direct light is blocked. Such a process is not straightforward due to the complicated reflection channels and weak amplitude of the received light signal. Although advanced techniques such as machine learning could be adopted to infer the data from the reflected light [49], the training cost is very high. People who host the VLC receivers could rotate their bodies or the receivers to avoid blockages [6]. However, such a method involves user interactions and might not be suitable for a static receiver. Instead, our proposed method of leveraging the side RF channels only needs to add a few small components to the receiver, making our solution cheaper, simpler, training-free, and without user intervention.

Strong ambient light. Ambient light can saturate the photodiode of the receiver. Various solutions have been proposed to solve the saturation issue [10, 32, 39]. For example, a narrow optical band-pass filter is used to only pass the light of intended frequency band [10], and a less sensitive photodetector or solar cells [32] are adopted to avoid being saturated when the ambient light is strong [39]. Although these methods mitigate the interference to some extent, they sacrifice the large visible light frequency band [10] or can only work when ambient light is not strong [39]. Our solution based on the side RF channel can provide VLC with the ability to work under any intensity levels of ambient light.

A hybrid design. Another solution to the blockage and saturation issues of VLC is a hybrid RF/VLC design [3, 30, 31], since the RF signal can penetrate blockages and is robust against ambient light. Compared to this solution, the proposed system has two advantages: i) It is transparent to VLC transmitters, and no modification is needed at the transmitter side; ii) The side RF channel does not interfere with commonly seen RF systems such as Wi-Fi, LTE, and Bluetooth.

10 CONCLUSION

In this paper, we exploit the side channels of VLC to tackle the blockage and saturation limitations of VLC. We modele the side channel and based on the model, we design a receiver that includes 1) a small and flexible coil to receive multiple overlapped side-channel signals and 2) a decoding method to decode the signals. We show that in MIMO VLC networks with blockage or strong ambient light interference, we could still receive and decode the VLC information from the side channel using a single receiver coil. We believe this work can stimulate follow-up works on dealing with the limitations of complex MIMO VLC networks and the design of new applications based on the side RF channel.

ACKNOWLEDGMENTS

We thank the anonymous reviewers and shepherd for their valuable comments. This work was partially supported by UMass Amherst Institute For Applied Life Sciences Equipment Fund.

REFERENCES

[1] ASTM. Standard B 258-02. 2014. Standard Specification for Standard Nominal Diameters and Cross-Sectional Areas of AWG Sizes of Solid Round Wires Used as Electrical Conductors. (2014).

[2] Trio Adiono and Syifaul Fuada. 2017. Optical interference noise filtering over visible light communication system utilizing analog high-pass filter circuit. In *Proc. of the 2017 Int. Symp. on Nonlinear Theory and Its Applications*. 616–619.

[3] Dushyantha A Basnayaka and Harald Haas. 2017. Design and analysis of a hybrid radio frequency and visible light communication system. *IEEE Transactions on Communications* 65, 10 (2017), 4334–4347.

[4] Jona Beysens, Ander Galisteo, Qing Wang, Diego Juara, Domenico Giustiniano, and Sofie Pollin. 2018. DenseVLC: A cell-free massive MIMO system with distributed LEDs. In *In Proceedings of the ACM Conference on emerging Networking EXperiments and Technologies (CoNEXT)*. 320–332.

[5] Jona Beysens, Qing Wang, Ander Galisteo, Domenico Giustiniano, and Sofie Pollin. 2020. A Cell-Free Networking System With Visible Light. *IEEE/ACM Transactions on Networking* (2020), 461–476.

[6] Jona Beysens, Qing Wang, and Sofie Pollin. 2019. Improving Blockage Robustness in VLC Networks. In *Proceedings of the IEEE International Conference on Communication Systems & Networks (COMSNETS)*. 164–171.

[7] Jona Beysens, Qing Wang, and Sofie Pollin. 2020. Exploiting Blockage in VLC Networks Through User Rotations. *IEEE Open Journal of the Communications Society* (2020), 1084–1099.

[8] Rui Bian, Iman Tavakkolnia, and Harald Haas. 2019. 15.73 Gb/s visible light communication with off-the-shelf LEDs. *Journal of Lightwave Technology* 37, 10 (2019), 2418–2424.

[9] Alexey Bodrov and Seung-Ki Sul. 2012. Analysis of wireless power transfer by coupled mode theory (CMT) and practical considerations to increase power transfer efficiency. In *Wireless Power Transfer-Principles and Engineering Explorations*. Intechopen.

[10] Charles J Carver, Zhao Tian, Hongyong Zhang, Kofi M Odame, Alberto Quattrini Li, and Xia Zhou. 2020. AmphiLight: Direct Air-Water Communication with Laser Light. In *Proceedings of the USENIX Symposium on Networked Systems Design and Implementation (NSDI)*. 373–388.

[11] Steve CQ Chen and Valerie Thomas. 2001. Optimization of inductive RFID technology. In *Proceedings of the IEEE International Symposium on Electronics and the Environment (ISEE)*. IEEE, 82–87.

[12] Hyunchae Chun, Ariel Gomez, Crisanto Quintana, Weida Zhang, Grahame Faulkner, and Dominic O'Brien. 2019. A Wide-Area Coverage 35 Gb/s Visible Light Communications Link for Indoor Wireless Applications. *Scientific reports* (2019), 1–8.

[13] Minhao Cui, Yuda Feng, Qing Wang, and Jie Xiong. 2020. Sniffing visible light communication through walls. In *Proceedings of the ACM International Conference on Mobile Computing and Networking (MobiCom)*. 1–14.

[14] John Cullerne, Valerie Illingworth, and John Daintith. 2000. *The Penguin dictionary of physics*. Penguin Group USA.

[15] Franco Di Paolo. 2018. *Networks and devices using planar transmissions lines*. CRC Press.

[16] 6G Flagship. 2019. Key Drivers and Research Challenges for 6G Ubiquitous Wireless Intelligence. (2019).

[17] A Galisteo, D Juara, and D Giustiniano. 2019. Research in Visible Light Communication Systems with OpenVLC1.3. In *Proceedings of the IEEE World Forum on Internet of Things (WF-IoT)*. 539–544.

[18] Ander Galisteo, Diego Juara, Qing Wang, and Domenico Giustiniano. 2018. OpenVLC1.2: Achieving higher throughput in low-end visible light communication networks. In *Proceedings of the IEEE Conference on Wireless On-demand Network Systems and Services (WONS)*. 117–120.

[19] Liane Grobe, Anagnostis Paraskevopoulos, Jonas Hilt, Dominic Schulz, Friedrich Lassak, Florian Hartlieb, Christoph Kottke, Volker Jungnickel, and Klaus-Dieter Langer. 2013. High-speed visible light communication systems. *IEEE communications magazine* 51, 12 (2013), 60–66.

[20] Jie Hao, Yanbing Yang, and Jun Luo. 2016. CeilingCast: Energy efficient and location-bound broadcast through LED-camera communication. In *Proceedings of the IEEE International Conference on Computer Communications (INFOCOM)*.

[21] Yang Hong, Tesi Wu, and Lian-Kuan Chen. 2016. On the performance of adaptive MIMO-OFDM indoor visible light communications. *IEEE Photonics Technology Letters* 28, 8 (2016), 907–910.

[22] Chin-Wei Hsu, Chi-Wai Chow, I-Cheng Lu, Yen-Liang Liu, Chien-Hung Yeh, and Yang Liu. 2016. High speed imaging 3× 3 MIMO phosphor white-light LED based visible light communication system. *IEEE Photonics Journal* 8, 6 (2016), 1–6.

[23] Norden Eh Huang. 2014. *Hilbert-Huang transform and its applications*. Vol. 16. World Scientific.

[24] Mohamed Sufyan Islim, Stefan Videv, Majid Safari, Enyuan Xie, Jonathan JD McKendry, Erdan Gu, Martin D Dawson, and Harald Haas. 2018. The impact of solar irradiance on visible light communications. *Journal of Lightwave Technology* 36, 12 (2018), 2376–2386.

[25] Aleksandar Jovicic, Junyi Li, and Tom Richardson. 2013. Visible light communication: opportunities, challenges and the path to market. *IEEE Communications Magazine* 51, 12 (2013), 26–32.

[26] Jie Lian and Maïté Brandt-Pearce. 2017. Multiuser MIMO indoor visible light communication system using spatial multiplexing. *Journal of Lightwave Technology* 35, 23 (2017), 5024–5033.

[27] Cen B Liu, Bahareh Sadeghi, and Edward W Knightly. 2011. Enabling vehicular visible light communication (V2LC) networks. In *Proceedings of the Eighth ACM international workshop on Vehicular inter-networking*. 41–50.

[28] Farshad Miramirkhani and Murat Uysal. 2017. Visible light communication channel modeling for underwater environments with blocking and shadowing. *IEEE Access* 6 (2017), 1082–1090.

[29] Quan Ngoc Pham, Vega Pradana Rachim, Jinyoung An, and Wan-Young Chung. 2017. Ambient light rejection using a novel average voltage tracking in visible light communication system. *Applied Sciences* 7, 7 (2017), 670.

[30] Yogi Salomo Mangontang Pratama and Kae Won Choi. 2018. Bandwidth aggregation protocol and throughput-optimal scheduler for hybrid RF and visible light communication systems. *IEEE Access* 6 (2018), 32173–32187.

[31] Michael B Rahaim, Anna Maria Vegni, and Thomas DC Little. 2011. A hybrid radio frequency and broadcast visible light communication system. In *2011 IEEE GLOBECOM Workshops (GC Wkshps)*. IEEE, 792–796.

[32] K Sindhubala and B Vijayalakshmi. 2017. Receiver intend to reduce ambient light noise in visible-light communication using solar panels. *Journal of Engineering Science & Technology Review* 10, 1 (2017).

[33] Faisal Tariq, Muhammad RA Khandaker, Kai-Kit Wong, Muhammad A Imran, Mehdi Bennis, and Merouane Debbah. 2020. A speculative study on 6G. *IEEE Wireless Communications* 27, 4 (2020), 118–125.

[34] Zhao Tian, Kevin Wright, and Xia Zhou. 2016. The DarkLight Rises: Visible Light Communication in the Dark. In *Proceedings of the ACM International Conference on Mobile Computing and Networking (MobiCom)*. 2–15.

[35] David Tse and Pramod Viswanath. 2005. *Fundamentals of wireless communication*. Cambridge university press.

[36] Dobroslav Tsonev, Stefan Videv, and Harald Haas. 2014. Light fidelity (Li-Fi): towards all-optical networking. In *Broadband Access Communication Technologies VIII*, Vol. 9007. International Society for Optics and Photonics, 900702.

[37] Purui Wang, Lilei Feng, Guojun Chen, Chenren Xu, Yue Wu, Kenuo Xu, Guobin Shen, Kuntai Du, Gang Huang, and Xuanzhe Liu. 2020. Renovating Road Signs for Infrastructure-to-Vehicle Networking: A Visible Light Backscatter Communication and Networking Approach. In *Proceedings of the ACM International Conference on Mobile Computing and Networking (MobiCom)*.

[38] Qing Wang, Domenico Giustiniano, and Daniele Puccinelli. 2014. OpenVLC: Software-defined visible light embedded networks. In *Proceedings of the ACM MobiCom workshop on Visible light communication systems*. 15–20.

[39] Qing Wang, Domenico Giustiniano, and Marco Zuniga. 2017. In light and in darkness, in motion and in stillness: A reliable and adaptive receiver for the internet of lights. *IEEE Journal on Selected Areas in Communications* 36, 1 (2017), 149–161.

[40] Qing Wang, Marco Zuniga, and Domenico Giustiniano. 2016. Passive communication with ambient light. In *Proceedings of the ACM International on Conference on emerging Networking EXperiments and Technologies (CoNEXT)*. ACM, 97–104.

[41] Enyuan Xie, Rui Bian, Xiangyu He, Mohamed Sufyan Islim, Cheng Chen, Jonathan McKendry, Erdan Gu, Harald Haas, and Martin D. Dawson. 2020. Over 10 Gbps VLC for Long-Distance Applications Using a GaN-Based Series-Biased Micro-LED Array. *IEEE Photonics Technology Letters* (2020), 499–502.

[42] Yanbing Yang, Jun Luo, Chen Chen, Zequn Chen, Wen-De Zhong, and Liangyin Chen. 2020. Pushing the Data Rate of Practical VLC via Combinatorial Light Emission. *IEEE Transactions on Mobile Computing* (2020), 1–1.

[43] Yanbing Yang, Jun Luo, Chen Chen, Wen-De Zhong, and Liangyin Chen. 2019. SynLight: Synthetic Light Emission for Fast Transmission in COTS Device-enabled VLC. In *Proceedings of the IEEE Conference on Computer Communications (INFOCOM)*. 1297–1305.

[44] Anil Yesilkaya, Ertugrul Basar, Farshad Miramirkhani, Erdal Panayirci, Murat Uysal, and Harald Haas. 2017. Optical MIMO-OFDM with generalized LED index modulation. *IEEE Transactions on Communications* (2017), 3429–3441.

[45] Kai Ying, Hua Qian, Robert J Baxley, and Saijie Yao. 2015. Joint optimization of precoder and equalizer in MIMO VLC systems. *IEEE Journal on selected areas in communications* (2015), 1949–1958.

[46] Kou Yoshida, Pavlos P Manousiadis, Rui Bian, Zhe Chen, Caroline Murawski, Malte C Gather, Harald Haas, Graham A Turnbull, and Ifor DW Samuel. 2020. 245 MHz bandwidth organic light-emitting diodes used in a gigabit optical wireless data link. *Nature Communications* (2020), 1–7.

[47] C Patrick Yue and S Simon Wong. 2000. Physical modeling of spiral inductors on silicon. *IEEE Transactions on electron devices* 47, 3 (2000), 560–568.

[48] Jialiang Zhang, Xinyu Zhang, and Gang Wu. 2015. Dancing with light: Predictive in-frame rate selection for visible light networks. In *Proceedings of the IEEE Conference on Computer Communications (INFOCOM)*. 2434–2442.

[49] Yonghe Zhu, Chen Gong, Jianghua Luo, Zhengyuan Xu, and Weiqiang Xu. 2019. SVM-Assisted Realization and Demonstration of Indoor 4 Mb/s Non-Line-of-Sight Visible Light Communication With Second-Order Reflection. *IEEE Photonics Journal* 11, 5 (2019), 1–17.